Multi-Timescale Analysis of the Spatial Representativeness of In Situ Soil Moisture Data within Satellite Footprints

Beatriz Molero, Dj Leroux, Philippe Richaume, Yh Kerr, Olivier Merlin, Mh Cosh, R Bindlish

AGU PUBLICATIONS

JGR

Journal of Geophysical Research: Atmospheres

RESEARCH ARTICLE
10.1002/2017JD027478

Key Points:
- The spatial representativeness of in situ stations tends to increase with the timescale within the satellite footprint
- Stations poorly represent the satellite footprint at subweekly scales, while either very well or poorly at seasonal scales
- The wavelet correlation (WCor) method is a useful tool to study the spatial scale mismatch between in situ and satellite observations

Correspondence to:
B. Molero,
beatriz.molero@cesbio.cnes.fr

Citation:
Molero, B., Leroux, D. J., Richaume, P., Kerr, Y. H., Merlin, O., Cosh, M. H., & Bindlish, R. (2018). Multi-timescale analysis of the spatial representativeness of in situ soil moisture data within satellite footprints. *Journal of Geophysical Research: Atmospheres*, *123*, 3–21. https://doi.org/10.1002/2017JD027478

Received 18 JUL 2017
Accepted 25 NOV 2017
Accepted article online 3 DEC 2017
Published online 4 JAN 2018
Corrected 23 JAN 2018

This article was corrected on 23 JAN 2018. See the end of the full text for details.

Multi-Timescale Analysis of the Spatial Representativeness of In Situ Soil Moisture Data within Satellite Footprints

B. Molero[1], D. J. Leroux[2], P. Richaume[1], Y. H. Kerr[1], O. Merlin[1], M. H. Cosh[3], and R. Bindlish[4]

[1]CESBIO (Centre d'Études Spatiales de la BIOsphère), Université de Toulouse, CNES, CNRS, IRD, UPS, Toulouse, France, [2]CNRM (Centre National de la Recherche Météorologique), Météo-France, CNRS, Toulouse, France, [3]USDA-ARS-Hydrology and Remote Sensing Laboratory, Beltsville, MD, USA, [4]NASA Goddard Space Flight Center, Greenbelt, MD, USA

Abstract We conduct a novel comprehensive investigation that seeks to prove the connection between spatial scales and timescales in surface soil moisture (SM) within the satellite footprint (~50 km). Modeled and measured point series at Yanco and Little Washita in situ networks are first decomposed into anomalies at timescales ranging from 0.5 to 128 days, using wavelet transforms. Then, their degree of spatial representativeness is evaluated on a per-timescale basis by comparison to large spatial scale data sets (the in situ spatial average, SMOS, AMSR2, and ECMWF). Four methods are used for this: temporal stability analysis (TStab), triple collocation (TC), percentage of correlated areas (CArea), and a new proposed approach that uses wavelet-based correlations (WCor). We found that the mean of the spatial representativeness values tends to increase with the timescale but so does their dispersion. Locations exhibit poor spatial representativeness at scales below 4 days, while either very good or poor representativeness at seasonal scales. Regarding the methods, TStab cannot be applied to the anomaly series due to their multiple zero-crossings, and TC is suitable for week and month scales but not for other scales where data set cross-correlations are found low. In contrast, WCor and CArea give consistent results at all timescales. WCor is less sensitive to the spatial sampling density, so it is a robust method that can be applied to sparse networks (one station per footprint). These results are promising to improve the validation and downscaling of satellite SM series and the optimization of SM networks.

1. Introduction

Soil moisture (SM) plays an important role in atmospheric, hydrologic, and ecological processes (Daly & Porporato, 2005; Legates et al., 2011; Rodriguez-Iturbe, 2000). By means of them, it participates at various scales, from the largest climatic and meteorological scales (Douville, 2004; Drusch, 2007) to the medium hydrological scale (Chen et al., 2011; Draper et al., 2012) and the smallest field and local scales (Vereecken et al., 2014).

The spatial scale of a set of spatially distributed SM measurements (or observations) refers to a triplet of entities: the extent (the area enclosing all the measurements), the spacing (the distance between measurements), and the support (the area actually sensed by the sensor or *resolution*; Blöschl & Sivapalan, 1995). A typical in situ station has a support of just some few centimeters (*point* or *local* support). In practice, it represents larger areas because the factors driving SM variability (vegetation, soil texture, topography, and rainfall) are spatially connected. This *effective support* or *spatial representativeness area* is defined by the surrounding area showing sufficient similarity with the station location in terms of SM, according to a given evaluation methodology. Hereafter, we will use simply *representativeness* to refer to *spatial representativeness*. From space, passive microwave sensors provide SM estimates at a global extent with a resolution of several tens of kilometers (*large* support), which is defined by the antenna footprint as the area containing half of the total signal power. C- and X-band sensors like AMSR-E, AMSR2, and WindSat (Mladenova et al., 2011; Parinussa et al., 2012; Wagner et al., 2007) and L-band sensors like SMOS and SMAP (Al Bitar et al., 2012; Colliander et al., 2017; Kerr et al., 2016) have shown good skills in capturing the temporal patterns of top-surface SM at ~1 cm and ~5 cm depths, respectively.

Factors driving SM variability (vegetation, soil texture, topography, and rainfall), although spatially dependent, are not homogeneous within satellite footprints. As a consequence, ground stations rarely represent satellite footprints perfectly. This *spatial scale mismatch* is by principle not known and difficult to estimate. Validation of satellite products usually consists of their direct comparison with in situ time series through

linear metrics (correlation, bias, and RMSE). Since the spatial scale mismatch is not considered, the statistics can be hampered to a great extent (Crow et al., 2012; Loew & Schlenz, 2011).

The spatial scale mismatch between satellite and in situ measurements can be reduced with upscaling approaches that increase the effective in situ support. They can be applied if multiple in situ stations are available within the footprint (dense networks). The simplest techniques consist of linear and weighted spatial averages of the stations time series (Jackson et al., 2010). The locations of the stations can also be selected in a spatial configuration that ensures the representativeness of the average, based on prior knowledge on, for example, soil texture and land cover (Bircher et al., 2012). Downscaling of satellite observations can potentially help in reducing the spatial scale mismatch for satellite validation (Malbéteau et al., 2016). The principal drawback of most upscaling and downscaling approaches is the difficulty to assess the method uncertainty and the remaining spatial scale mismatch. When the statistical spatial structure of SM can be inferred, the upscaling uncertainty can be estimated with geostatistical techniques like block kriging (J. Wang et al., 2015). However, they need dense sampling schemes ($>$100; Webster & Oliver, 1992) that could never be met in practice for long-term in situ networks.

An alternative approach is to choose directly the ground station that behaves most like the footprint time series. Temporal stability analysis (Vachaud et al., 1985) selects the station that exhibits the smallest difference, in terms of mean and dispersion (Cosh et al., 2006, 2008; Kornelsen & Coulibaly, 2013). It is based on the assumption that spatial SM fields are stable in time, which is not always true (Yee et al., 2016). Triple collocation (TC) can also be used to estimate the representativeness of ground stations (Chen et al., 2016; Gruber et al., 2013; Miralles et al., 2010). It requires three data sets and is very sensitive to the independence between the errors and between the signals and the errors (Yilmaz & Crow, 2014). Finally, the "inverse footprint" method (Nicolai-Shaw et al., 2015; Orlowsky & Seneviratne, 2014) simply evaluates the synchronism between surrounding stations.

The spatial representativeness of SM data sets may be different depending on the timescale. Studies at country and continental extents showed that large and small timescales have large and small representativeness areas, respectively (Cayan & Georgakakos, 1995; Entin et al., 2000; Vinnikov et al., 1996). Entin et al. (2000) identified two spatiotemporal scales: the small scale was of the order of some tens of meters and few days and was due to local processes such as infiltration, precipitation, and drainage; the large scale was of the order of some hundreds of kilometers and 2–3 months and was due to climatic atmospheric forcing. The works of Chaney et al. (2014) and Su and Ryu (2015) have provided similar conclusions for footprint extents. Chaney et al. (2014) showed that in the Little River catchment, large spatial scale factors (land cover and evapotranspiration) influence SM seasonal cycles, while the small ones (soil texture) do not. Similarly, Su and Ryu (2015) have showed that the correlation between point and large-support data sets (in situ and satellite) increases with the timescale. However, at the view of the literature on TC, we ascertain an alternative interpretation about SM seasonal scales. TC studies have usually considered that there exist significant differences between the seasonal components or "climatologies" of ground and satellite/model data sets due to their different spatial support sizes (Gruber et al., 2016). For this reason, TC studies have systematically detrended the SM series for the seasonal component. To our knowledge, this apparent divergence between interpretations of the seasonal SM component has not been addressed yet in the literature.

The evaluation of SM representativeness on a per-timescale basis requires separating the SM series in timescales. Moving averages have been applied to separate the seasonality and trend components (large timescales) from the anomaly series component (shorter timescales; Gruber et al., 2013; Nicolai-Shaw et al., 2015). Although events are localized with precision in the anomaly series, these are still affected by part of the seasonal component. Fourier analysis has been used to analyze the power of each timescale (Katul et al., 2007; Su et al., 2016), but it does not allow localizing events in time. More advanced spectral techniques like the short-time Fourier transform and wavelet transforms can solve this issue. Wavelet transforms have the advantage of localizing events in time with a precision that does not depend on the timescale (Barford et al., 1992; Cornish et al., 2006). Some examples of wavelets applied to SM series include the study of daily to annual components at different depths (Lauzon et al., 2004), the connections with other geophysical variables per timescale (Graf et al., 2014), and the correction of multiplicative and additive biases per timescale (Su & Ryu, 2015).

The objective of this study is to investigate the connection between spatial and timescales within satellite footprints. The investigation is performed in three steps: First, a preliminary assessment of the scales and their geophysical drivers is conducted on modeled SM data. Second, we investigate which method is suited the best for assessing spatial representativeness (spatial scale) when SM time series are decomposed in timescales. Timescales are obtained with wavelet transforms. The approaches tested for assessing the spatial representativeness are temporal stability, triple collocation, and two new ones: the temporally correlated areas (CArea) method and an approach based on wavelet correlations (WCor). The third and final step consists of analyzing actual measured SM data to verify the conclusions reached at that point. To our knowledge, this is the first study of this kind to investigate the footprint extent with a comprehensive set of methods and data sets. In addition, we analyze the seasonal components of point and footprint support series in order to solve the apparent divergence in literature mentioned before.

This article is structured as follows. Section 2 presents the methods used for the analyses in the time domain (wavelets; section 2.1) and in the spatial domain (representativeness methods; section 2.2). Section 3 describes the data sets. Section 4 gathers the results from each of the three steps of the investigation in respectively three subsections. The conclusions are summarized in section 5.

2. Materials and Methods

2.1. Timescale Decomposition of SM

Wavelets are mathematical functions that can be used to decompose time series in a set of timescales (Foufoula-Georgiou & Kumar, 1994; Percival & Walden, 2000). Wavelet transforms are time-frequency transforms: they detect the frequency components of the signal and also when events occur in time. The continuous wavelet transform is expressed as a collection of variables $\{W(\tau, t): \tau > 0, -\infty < t < \infty\}$, where τ denotes the timescale (equation (1)). It consists of convoluting the original signal $x(t)$ with a set of translated and stretched/shrinked versions of the wavelet basis function $\psi(t)$.

$$W(\tau,t) = \int_{-\infty}^{\infty} x(u)\psi\left(\frac{u-t}{\tau}\right)\mathrm{d}u \tag{1}$$

The maximal overlap discrete wavelet transform (MODWT) is a subsampled version of the continuous wavelet transform at dyadic scales (equation (2)):

$$\tau_j = 2^{j-1}T_s, \quad j = 1 \ , \ 2 \ , \ \ldots \ , \ \mathrm{J0} \tag{2}$$

where J0 is the last level of decomposition, T_s is the sampling period of the original signal (in time units), τ_j is the timescale (in time units), and j is the the unit-less scale. The maximal overlap discrete wavelet transform can be applied to any sample size and is shift-invariant (Percival & Walden, 2000, pp. 159, 160).

The wavelet transform produces J0 series of *wavelet* coefficients $\{W_j(t)\}$ for the scales $\{\tau_j\}$ ($j = 1, 2, \ldots, \mathrm{J0}$) and one series of *scale* coefficients $V_{\mathrm{J0}}(t)$ that contains all variations at scales larger than τ_{J0}. For the sake of clarity, the scale series are usually referred as V_{J0} instead of $W_{(\mathrm{J0}\ -\ \infty]}$. The inverse transform of the W_j and V_{J0} coefficients produces the *detail* (D_j) and *smooth* (S_{J0}) series, respectively. The detail series represent anomalies at scale τ_j (rapid variations), that is, differences in weighted averages of periods of length τ_j or *slightly longer* (Percival & Walden, 2000, pp. 11 and 59). They are zero mean by construction. The smooth series contain the remaining variations and the bias for timescales larger than J0 (slow variations). The sum of the detail and smooth series recovers the original time series (equation (3)):

$$x(t) = \sum_{j=1}^{\mathrm{J0}} D_j + S_{\mathrm{J0}} \tag{3}$$

One of the critical aspects of wavelet analysis is the choice of the maximum level of decomposition J0 and the wavelet basis function $\psi(t)$. The largest timescale at J0 should be smaller than the length of the series ($2^{\mathrm{J0}\ -\ 1} < N$). In this study, we use 6 month and 2 year series with a sampling period (T_s) of half a day. Therefore, we select J0 = 8 for the 6 month series and J0 = 9 for the 2 year series. The list of possible scales is provided in Table 1. Regarding the wavelet basis function, we will use the Daubechies-4 (D4; Daubechies, 1992) and the Haar (Haar, 1910) wavelet. While D4 better isolates timescales due to its sharper response in the frequency domain, it is longer in time than Haar. Given that the length of the wavelet at scale J0 should be

Table 1
Wavelet Scales for Sampling Period T_s = 0.5 Days

Timescale	Timescale (days)
j	$\tau_j = 2^{j-1} \cdot T_s$
1	0.5
2	1
3	2
4	4
5	8
6	16
7	32
8	64
9	128

shorter than the length of the series (Cornish et al., 2006), we select Haar for the 6 month series and D4 for the 2 year series.

2.2. Spatial Representativeness Metrics

In this section, we describe the methods we use to evaluate the spatial representativeness: two existing methods, temporal stability (TStab) and triple collocation (TC), and two new methods, the temporally correlated area (CArea) and the wavelet-based correlation (WCor). CArea is designed to serve as the reference when working with modeled spatial fields since it accounts for all the local supports contained within the footprint. In the case of dense in situ networks, the spatial sampling is insufficient to ensure accurate CArea results. WCor is designed to serve as an alternative method to TStab and TC that, as will be shown, require quite restrictive conditions constraining their use to limited range of timescales.

2.2.1. Temporal Stability (TStab)

TStab was introduced by Vachaud et al. (1985) and has been thoroughly detailed in a number of publications (Cosh et al., 2006; Martínez-Fernández & Ceballos, 2005; Mittelbach & Seneviratne, 2012). In short, TStab evaluates how the relative differences (RD_{i0}; equation (4)) between the spatial average values SM_{avg} and point support values SM_{i0} at the location i_0 vary in time. The most representative point time series is the one with both smaller mean RD (MRD_{i0}; equation (5)) and smaller standard deviation of RD ($SDRD_{i0}$; equation (6)). In this study, stations with small and big MRD also had small and big SDRD, respectively (not shown here). Thus, for the sake of concision, we bring the two metrics into one, the $RMSE_{i0}$ (equation (7)), following the notation of Jacobs et al. (2004):

$$RD_{i0}(t) = \frac{SM_{i0}(t) - SM_{avg}(t)}{SM_{avg}(t)} \tag{4}$$

$$MRD_{i0} = \frac{1}{N}\sum_{t=1}^{N} RD_{i0}(t) \tag{5}$$

$$SDRD_{i0} = \sqrt{\frac{1}{N-1}\sum_{t=1}^{N}\left(RD_{i0}(t) - MRD_{i0}\right)^2} \tag{6}$$

$$RMSE_{i0} = \sqrt{MRD_{i0}^2 + SDRD_{i0}^2} \tag{7}$$

2.2.2. Triple Collocation (TC)

TC is a technique for estimating the random errors of three collocated data sets that are meant to represent the same geophysical variable (Stoffelen, 1998). It relies on a linear error model:

$$x_k(t) = \alpha_k + \beta_k\theta(t) + \varepsilon_k(t) \tag{8}$$

where k denotes one of the three data sets, α_k and β_k are calibration constants, $\theta(t)$ is the (unknown) true SM, and ε_k is the error term. In the case of SM, when TC is used to evaluate the spatial representativeness, the TC triplet is formed by the in situ data set (which is assessed for representativeness) and two data sets of equivalent large supports. Supposing that the latter show stronger similarities because of their similar support sizes and that the data set' errors are much smaller than the differences due to the spatial scale mismatch, the error metrics of the in situ data set should mainly reflect its spatial representativeness (Gruber et al., 2016; Vogelzang & Stoffelen, 2012).

Two TC metrics are typically used to assess the errors of each dataset x_k, the variance of its errors $\sigma^2_{\varepsilon_k}$ (Gruber et al., 2013; Miralles et al., 2010) and its correlation with the true soil moisture $\rho_{x_k,\theta}$ or $\rho_{x_k,\text{true}}$ for readability (Chen et al., 2016; McColl et al., 2014). In this study we use the TC correlation coefficient because, unlike the error variance, it is normalized by the total signal power and so allows the direct comparison of results from different stations and networks.

Assuming that the covariances between the true signal $\theta(t)$ and the errors $\varepsilon_k(t)$ and between the errors of different data sets are null, the error variance and the TC correlation estimators can be derived (Chen et al., 2016) and written as

$$\sigma^2_{\varepsilon_k} = \sigma^2_k - \sigma_{kl}\sigma_{km}/\sigma_{ml} \tag{9}$$

$$\rho_{x_k,\text{true}} = \pm\sqrt{\frac{\sigma_{kl}\sigma_{km}}{\sigma^2_k\sigma_{ml}}} \tag{10}$$

where σ^2_k is the variance of data set k and σ_{kl}, σ_{km}, and σ_{ml} are the cross-covariances between the two data sets specified in the subscript. The three following conditions are necessary to compute equation (10) (Chen et al., 2016): (a) nonnegative cross-correlation between all data sets; (b) nonnegative $\sigma^2_{\varepsilon_k}$; and (c) nonnegative $\rho^2_{x_k,\text{true}}$.

2.2.3. Temporally Correlated Areas (CArea)

Nicolai-Shaw et al. (2015) and Orlowsky and Seneviratne (2014) introduced the notion of "inverse footprint" for in situ SM series that they define as the area surrounding a station where other stations exhibit temporal similarity (correlation) above a specified threshold. In this study, we propose a modification that we call the *temporally correlated areas* (CArea) method. The three main changes are as follows:

1. It is only applied to SM gridded data. Even in the case of dense in situ networks, the spatial sampling is too sparse for detailed spatiotemporal analyses.
2. Pearson correlation replaces Spearman correlation, in order to be consistent with the other approaches used that rely on the Pearson statistic.
3. The final metric is the percentage of pixels above a specific correlation threshold. The mathematical formula is presented in equation (11), where i_0 is the location where representativeness is evaluated, M is the number of locations i within the area A, $R_{x_i,x_{i_0}}$ is the correlation between the SM time series at locations i and i_0, R_{th} the correlation threshold, and H the Heaviside function that is 0 and 1 for negative and positive numbers, respectively.

$$\text{CArea}_{i0} = \frac{1}{M}\sum_{\forall i \neq i_0 \subset A} H\left(R_{x_i,x_{i_0}} - R_{\text{th}}\right) \times 100\ (\%) \tag{11}$$

The CArea method consists then of calculating the percentage of point SM time series within the study area that correlate with the reference series x_{i0} above a specific threshold. The higher the percentage (and the correlation threshold), the more representative is a location i_0.

2.2.4. Wavelet-Based Correlation (WCor)

WCor evaluates the representativeness of a location i_0 on a per-timescale basis. First, the point time series and the large-support series at that location are decomposed in detail series with wavelet transforms. Then, correlation R_j between the detail series at each scale j is computed:

$$R_{i_0,j} = R\left\{D_j^{\text{point}-i0}, D_j^{\text{large}}\right\},\ \ j = 1\ ,\ \ 2\ ,\ \ \ldots J0 \tag{12}$$

The WCor values are simply a measure of linear matching. They cannot by themselves quantify separately the errors in the data sets and the spatial scale mismatch. However, the analysis of a collection of in situ and modeled SM series in the following sections will show that they are useful to understand the connection between spatial and temporal scales and to compare the relative representativeness levels of a set of stations.

3. Data Sets

3.1. Local-Support Data Sets

We have selected for analysis the Little Washita watershed in USA (Cosh et al., 2006) and the Yanco area of the Murrumbidgee Soil Moisture Monitoring Network in Australia (Smith et al., 2012). They are selected because both are monitored by dense in situ networks and have contrasting climatic conditions (subhumid and semiarid, respectively) and SM forcing (irrigation is present in Yanco but not in Little Washita). Little Washita will be used for the analysis of point in situ and point modeled series and Yanco for the analysis of time series of modeled SM gridded data at 1 km resolution. As explained in the introduction, modeled data will be used for illustrating the connections between spatial scales, timescales, and geophysical variables, while actual measured data will be used for verifying the findings.

Table 2
Values Assigned to the Pan's Model Parameters for the Generation on Synthetic SM Time Series

Parameter	Value	Differences with Pan et al. (2003)
γ	0.40	Adjusted to control the effect of p ($\gamma = 1$ produced SM > 1 m^3/m^3)
SM_{min} (m^3/m^3)	0.025	
SM_{max} (m^3/m^3)	0.5	
η (m/yr)	$\eta(t) =$ max $\{0.2 \cdot Ks + 0.4 \cdot LAI(t), 0.5\}$	Equation changed to match observations
Z (m)	$Z = Z_{max} - r_{mod} \cdot (Ks - Ks_{min})$ with $r_{mod} = \frac{Z_{max}-Z_{min}}{Ks_{max}-Ks_{min}} = \frac{0.09-0.025}{5-0.05}$	Equation changed to match observations. A texture-depending Z allows a wider range of decay rates. Z is reduced as soil becomes sandier (smaller depth provokes faster changes)
Ks (cm/h)	Sand: Ks = 5, loam: Ks = 1.3	Source: FAO http://ftp.fao.org/fi/cdrom/fao_training/FAO_Training/General/x6706e/x6706e09.htm

The Little Washita network has an extent of ~610 km^2. The average annual rainfall is 750 mm, and most of it takes place in spring and autumn (Allen & Naney, 1991). The area is mainly covered by rangeland and crops, soil texture is diverse (sands, loams and clays), and the topography is moderately rolling. The network is made up of 20 permanent Stevens Hydra Probe stations installed at a depth of 5 cm with a sensing range between 3 and 7 cm.

The Yanco network has an extent of ~3,000 km^2. The average annual rainfall is around 400 mm with precipitations concentrated in winter and spring. The area is mainly flat and is covered by pastures and both dry and irrigated crops. The network is made up of 13 permanent Stevens Hydra Probe stations providing SM integrated over the top 5 cm of soil.

3.1.1. Modeled Series (Little Washita)

The model in Pan et al. (2003) was specifically designed for the Little Washita network. Simplicity is its major asset, and the output SM time series are adequately realistic for our purposes. Three components with distinctive temporal scales control the SM series dynamics: precipitation (short-term), texture (short-to-medium term), and vegetation (seasonal term). These timescales could be represented by other factors in other areas of study or in more complex models. For this reason, we consider that precipitation includes irrigation, texture represents any soil memory process, and vegetation represents any seasonal signal, like temperature trends.

The model is summarized by the following equation:

$$SM(t) = \min\left\{ \max\left\{ SM(t-1)\cdot e^{\frac{-\eta(t)\cdot Ts}{Z}} + \frac{\gamma \cdot p(t)}{\eta(t)\cdot Ts}\cdot\left[1 - e^{\frac{-\eta(t)\cdot Ts}{Z}}\right], SM_{min}\right\}, SM_{max}\right\} \quad (13)$$

where T_s is the sampling period in hours (h), $p(t)$ is the cumulative precipitation (m) between $t-1$ and t, γ is the interception by vegetation, η is the loss coefficient (m/h), and Z is the penetration depth (m). The loss coefficient is calculated as a function of the drainage coefficient Ks and the leaf-area index (LAI). The parameters used in this study are described in Table 2.

Two-year SM series are produced with this model at a 12 h sampling interval. Two sets of series (a, b) are generated by varying the LAI amplitude. Each set is formed by a reference series (ref-a/ref-b) and four sample series (1-, 2-, 3-, 4-a/b). The reference series are produced for a loam texture using the in situ measured precipitation and the MODIS LAI time series observed at station 1. The ref-a time series is shown in Figure 1a, together with the true in situ series at station 1. Sample series are generated identically to their respective reference series except for one variable (Table 3): For sample series 1-a/b, we introduced random variations in precipitation amplitudes. For sample series 2-a/b, we changed also the synchronization of some precipitation events (10% of the events are randomly selected and shifted in time by +0.5 day and another 10% by −0.5 day). For series 3-a/b,

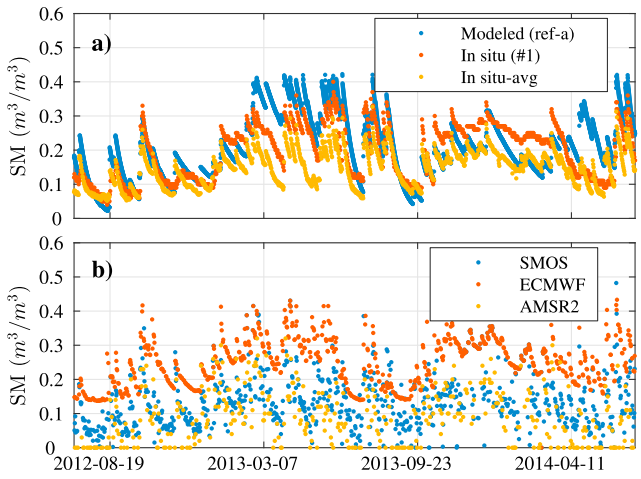

Figure 1. Time series of the SM data sets used in the Little Washita region, before gap filling. Only one of the time series of the modeled data set (ref-a) and two of the in situ data set (station 1 and the spatial average) are included.

Table 3
Characteristics of the Modeled SM Series of Little Washita

	Variables		
Series	Precipitation	Texture	LAI
Ref-a/b	$p_{ref}(t)$	Loam	LAI_{ref-a},$LAI_{ref-b} = LAI_{ref-a}/4$
1-a/b	*Different amplitudes* $p(t) = p_{ref}(t) + N(0, \sigma_{p_{ref}}/4)$	Loam	$LAI_{ref-a/b}$
2-a/b	*Different amplitudes and times: 10% of the events shifted by +0.5 day and 10%, by −0.5 day* $p(t) = p_{ref-SHIFT}(t) + N(0, \sigma_{p_{ref}}/4)$	Loam	$LAI_{ref-a/b}$
3-a/b	$p_{ref}(t)$	*Sand*	$LAI_{ref-a/b}$
4-a/b	$p_{ref}(t)$	Loam	*1 month shift* $LAI_{a/b}(t) = LAI_{ref-a/b}(t-30)$

we changed the texture to sand. Finally, for series 4-a/b, we introduced a 30 day time shift in the seasonal component. The detailed setup is provided in Table 3, where the variable changes are highlighted in italics.

3.1.2. In Situ Series (Little Washita)

The 20 in situ series of Little Washita for the 2 year period from July 2012 to July 2014 are selected. The data was provided by the team of the U.S. Department of Agriculture (USDA) in charge of maintaining the network. Data access and contact details can be found in the USDA Agricultural Research Service website (http://ars.mesonet.org/). The spatial average of all the station series and the time series measured at station 1 are shown for illustration in Figure 1a. Since wavelet transforms need regularly sampled time series, big gaps (>1 month) are filled by linear regression with the most similar station series. The percentage of filled gaps with this method is ~5.7% of the entire series. The remaining gaps, which represent ~1.1% of the samples, are filled with a discrete cosine transform (DCT) approach (G. Wang et al., 2012). The advantage of DCT is that it uses the full series—and not just local information—to estimate the missing data based on the signal spectrum.

3.1.3. In Situ DISPATCH Gridded Data (Yanco)

In this study, SM maps at 1 km resolution are generated by disaggregating the spatial average of the SM in situ Yanco time series. Yanco in situ data are available from the OzNet hydrological monitoring network website (http://www.oznet.org.au/). The disaggregation method used is derived from the operational version of the Disaggregation based on Physical and Theoretical Scale Change (DISPATCH) algorithm (Merlin et al., 2012, 2013; Molero et al., 2016). Former validation studies of DISPATCH over the Yanco region gave satisfactory results (Malbéteau et al., 2016; Merlin et al., 2012). The algorithm was originally designed to improve the resolution of satellite SM data sets by using temperature and vegetation data from optical/thermal sensors like MODIS. Note that in this study, we replace the satellite SM by the Yanco in situ average series, so that the SM maps are as close as possible to the ground reality. DISPATCH preserves the spatial average by construction. The data set will be called in situ DISPATCH (in situ-DIS).

The Yanco in situ-DIS series are sampled at SMOS overpass times (approximately 6 A.M. and 6 P.M.). Long periods of clouds reduced dramatically the availability of DISPATCH data during the Austral winter; as an example, most of the in situ-DIS series at the stations' locations presented long periods of unavailability (1–2 months), and data gaps represented 50% of the series in average. As a consequence, we only consider the 6 months from September 2014 to March 2015, which are affected by much shorter periods (below 9 days) and lower percentages of unavailability (~23%). Data gaps are filled with the DCT approach (G. Wang et al., 2012).

3.2. Large-Support Data Sets

3.2.1. SMOS

The SMOS mission (Kerr et al., 2001) is led by the European Space Agency (ESA) with collaboration of the Centre National d'Etudes Spatiales and the Centro Para el Desarrollo Tecnológico Industrial. The SMOS sensor is a passive 2-D microwave interferometer observing the Earth at L-band (1.4 GHz) dedicated for the observation of SM and ocean salinity. The mission provides SM estimates in m^3/m^3 over the top ~5 cm surface layer. The footprint (support) has a resolution that varies from 27 to 55 km depending on the observation geometry, with an average resolution of 43 km. The maximum revisit time of SMOS is 3 days with crossing nodes at 6 A.M. and 6 P.M. local solar time for ascending and descending orbits, respectively.

The SMOS data used in this study are obtained from the ESA Level 2 (L2) SM products (version 620). The SM retrieval algorithm takes into account the landscape heterogeneity of the observed surface. When the dominant land cover is low-vegetated soil (like in this study), the brightness temperatures of the low-vegetated part are modeled with the L-band Microwave Emission of the Biosphere forward model (L-MEB) (Wigneron et al., 2007). Details of the L2 SM retrieval algorithms can be found in Kerr et al. (2012, 2014).

The L2 grid nodes that are in the center of each in situ network are selected: the node 226157 for Little Washita and the node 8174767 for Yanco. These are depicted in Figure 2, together with the position of the ground stations of each network. Ascending and descending orbits are merged in one single time series with a 0.5 day sampling period. The original SMOS time series for the Little Washita network is shown in Figure 1b. SM retrievals with probability of radiofrequency interference (DQX) higher than 10% and data quality index (DQX) higher than 20% are removed. The gaps represent 59% of the Little Washita and Yanco SMOS series and are evenly distributed: the mean number of consecutive gaps is 2.8, and the mean number of consecutive samples (without gaps) is 2.2. They are filled with the DCT method.

3.2.2. AMSR2

The Advanced Microwave Scanning Radiometer 2 (AMSR2) is a passive multiband scanning radiometer onboard the Global Change Observation Mission Water 1 (GCOM-W1) satellite, launched by the Japan Aerospace Exploration Agency in May 2012. Its revisit time is 1–2 days with crossing nodes at 1:30 P.M. and 1:30 A.M. local solar time for ascending and descending orbits, respectively. Since SM derived from lower frequencies is expected to be more accurate, the lowest AMSR2 band (6.9 GHz, C-band) is selected here. At this frequency, the footprint is ~35 × 61 km (along scan × along track; Japan Aerospace Exploration Agency, 2013), and the derived SM products represent the soil moisture of the top ~1–2 cm surface layer.

Several AMSR2 SM products exist. We use the Land Parameter Retrieval Model (LPRM) products (Owe et al., 2008). LPRM considers the surface as homogeneous within the footprint in terms of vegetation scattering albedo, surface roughness, and so on. The product distributed by the NASA Goddard Earth Sciences Data and Information Services Center showed unusual temporal patterns and positive biases (Cho et al., 2017), so we use an AMSR2-LPRM SM data set directly provided by Dr. Parinussa.

We only used LPRM products from descending overpasses (1:30 A.M.). They have been proved as more accurate than their ascending counterparts (Draper et al., 2009; Lei et al., 2015), probably due to the more uniform surface temperature and soil moisture vertical profiles. For each network in this study, the AMSR2 pixel closer to the selected SMOS node is chosen (Figure 2). The AMSR2 time series for the Little Washita network is shown in Figure 1b. SM estimates are discarded either when they are equal to zero or when the quality mask values are higher than 68. On average, gaps represent 70% of the AMSR2 series and are uniformly distributed along the Little Washita and Yanco series: the mean number of consecutive gaps is 3.8 and 1.9, respectively, and the mean number of consecutive samples is 1. Data gaps are filled with the DCT method.

3.2.3. ECMWF

We use the ECMWF SM data set used by the SMOS L2 processor as initial guess in the retrieval loop. This custom ECMWF data set is obtained from the top 0–7 cm soil layer of the ECMWF forecast system and has been interpolated in space and time to match the SMOS L2 grid and overpass times. The custom ECWMF product is extracted from the SM_Init_Val field of the Level 2 Soil Moisture Data Analysis Product (MIR_SMDAP2), which is available through the ESA SMOS dissemination web service (https://smos-ds-02.eo.esa.int/oads/access/). More information on the ECMWF auxiliary product can be found in Kerr et al. (2012, 2014, 2016). The ECMWF time series for the Little Washita network is shown in Figure 1b. On average, gaps represent 48% of the series and are uniformly distributed: the mean number of consecutive gaps is 2.5, and the mean number of consecutive samples (without gaps) is 2.7. Gaps are filled with the DCT method.

4. Results and Discussion

4.1. Connection Between Spatial and Timescales

This section presents the first step of our investigation and seeks to reveal the existing connections between spatial scales, timescales, and geophysical drivers in SM modeled data sets. We analyze how SM timescales are influenced by differences in the sources of SM variability (forcing events, soil memory, and seasonal sources), for which the Little Washita modeled series were specifically designed. To this end, we evaluate the correlation between each sample series and its respective reference series (*a* or *b*, Table 3) on a per-timescale basis.

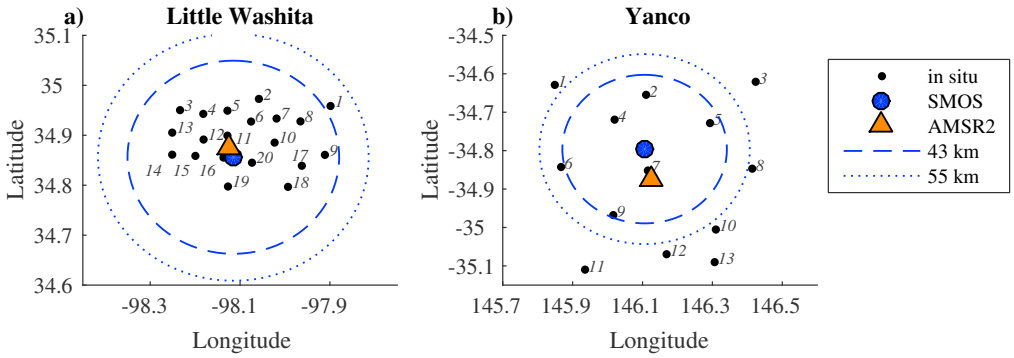

Figure 2. Location of the in situ stations and the SMOS and AMSR2 grid nodes in each of the validation areas. The circles represent two typical SMOS antenna footprint sizes considered in the retrieval algorithms: the average one of 43 km diameter and the maximum one of 55 km diameter.

The correlation of each sample–reference series pair is depicted in Figure 3 with differently colored lines. Solid lines correspond to correlations of the *a* group and dashed lines to the *b* group. Differences in forcing events (blue and red lines) deteriorate the correlation, at least in the first timescales (≤2 days). Moreover, desynchronizations produce irregular correlation patterns (red lines). Regarding texture heterogeneity (magenta lines), it deteriorates the correlations of middle scales up to the first seasonal scale (32 to 64 day scales). This illustrates that both meteorological forcing and surface memory can contribute to the month and seasonal scale signatures. Finally, when the seasonal component is not synchronized, the correlation at month and seasonal scales is hampered. This happens only when the seasonal component represents an important part of signal (case 4-a); otherwise, the correlation is maintained (case 4-b).

We have just shown the connections between some of the sources of SM variability and SM timescales, from a model perspective. Do these sources also exhibit characteristic spatial scales? For an exhaustive spatial investigation, the area under study requires to be fully sampled, so in the next experiment, we use the time series of in situ-DIS spatialized data. We evaluate the spatial representativeness of the pixels containing an in situ station on a per-timescale basis, by applying CArea to their wavelet decomposed series. We also evaluate the representativeness of two other series that are expected to represent the satellite footprint better than the point in situ series: the field average series (FAvg, the average of all the pixels) and the network average series (NAvg, the average of the pixels containing a station).

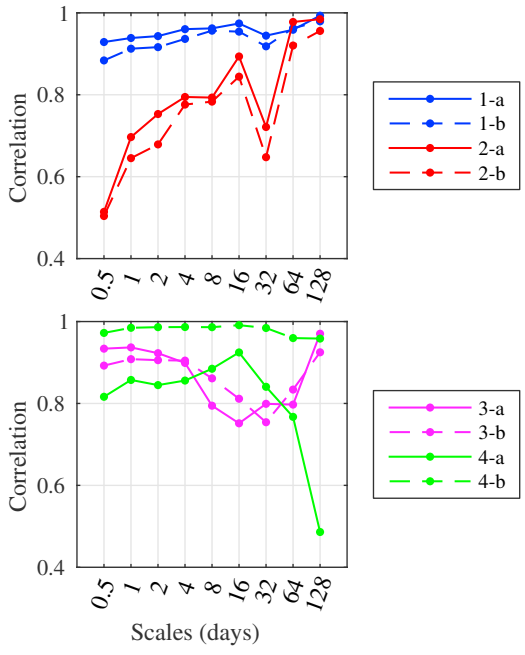

Figure 3. Correlations between the detail series of different sample series and their respective reference series (a or b), as a function of timescales.

The results are presented in Figure 4, where each line represents the CArea values obtained for a specific pixel for a range of correlation thresholds. Regardless of the FAvg and the NAvg series that have their own names, the ID of each pixel corresponds to the ID of the in situ station contained within. We observe that the lines move to the right and are more distant from each other as the timescale increases. This implies that, in general, spatial representativeness increases with the timescale, but the evolution is not the same for all locations. The latter could be explained by the combination between the propagation of small-scale effects and the appearance of larger scale SM factors (the propagation of small-scale effects was shown in the modeled Little Washita series). As expected, the field and the network average series are the most representative ones at all timescales.

Small timescales (0.5–2 days) exhibit the smallest correlated area, with less than 25% of the area correlated above 0.5 (Figure 4). This can be due to three possible reasons: (i) gap filling, (ii) noise from the disaggregation method and inputs, and (iii) important spatial heterogeneity. In

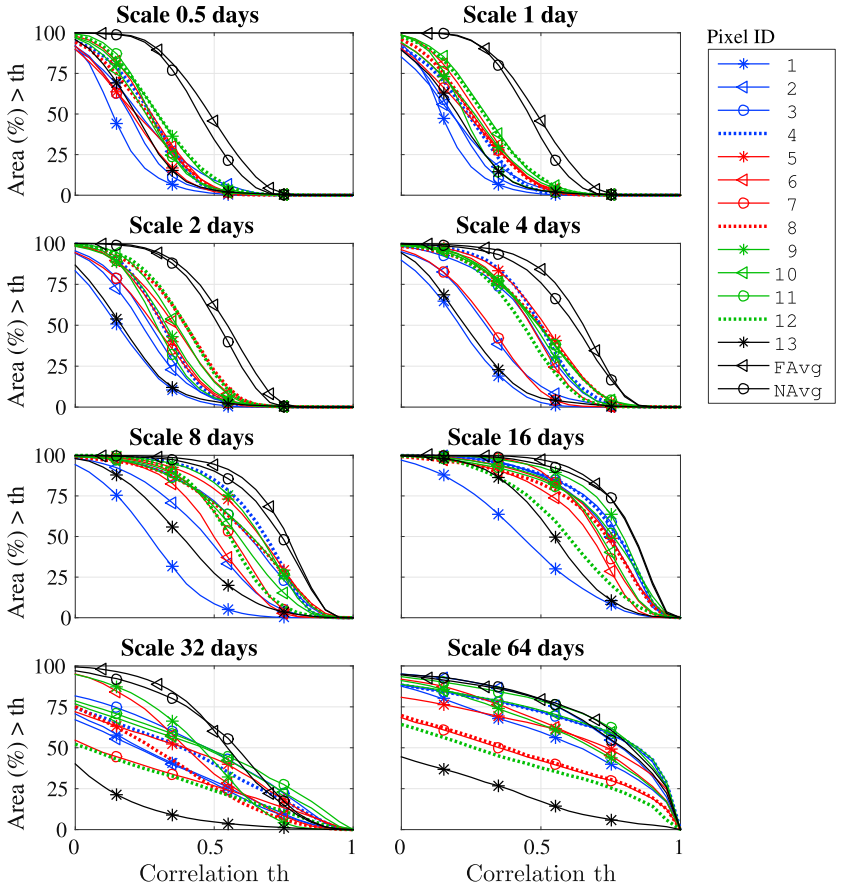

Figure 4. CArea scores: Size of the representativeness area in percentage of the total area, for a set of different locations (pixels) and the field and network average series (FAvg, NAvg). The data set is the in situ-DIS Yanco data set, for the 6 month period from September 2014 to March 2015.

order to assess the impact of gap filling, we used measured in situ series, where we could set the same gaps as those in the in situ-DIS series and compare scores before and after filling the gaps. Since the number of spatial samples was not large enough for applying CArea (13 stations), we simply computed the wavelet correlation scores. We found that, at the 0.5–2 day scales, correlation decreased by 0.08 on average. This means that gap filling does not change significantly the first three timescales as shown in Figure 4, with respect to the other timescales. Concerning the disaggregation noise, we expect it to be negligible with respect to the geophysical heterogeneity because the analysis of actual in situ series, as it will be shown in section 4.3, exhibited similar decorrelation levels. Hence, we may conclude that the spatial heterogeneity is the main cause of low correlation at subweekly timescales. In this case, the heterogeneity is most likely controlled by irrigation: the Yanco area contains both irrigated and nonirrigated plots, and we showed before that precipitation (and by extension, irrigation) produced decorrelation at short timescales.

Regarding weekly scales (8–16 days), most of the series have more than 50% of the surface correlated above 0.5 and 0.6 correlation points, respectively. This suggests that there is little soil heterogeneity, according to our analysis of Figure 3 where texture was associated to middle scales. The month scale (32 days) breaks the tendency of increasing representativeness with timescale. As we deducted from Figure 3, such drops in correlation appear at similar timescales when precipitation events are not synchronized, a phenomenon that should be present in Yanco because of irrigation. Also taking into account that the 32 day scale has small temporal variance, similar to that of the 2 day scale for this data set (not shown here), the signal-to-noise ratio might be quite low and induce low correlation (as demonstrated by Berger & Sweney, 1965; Goodwin & Leech, 2006).

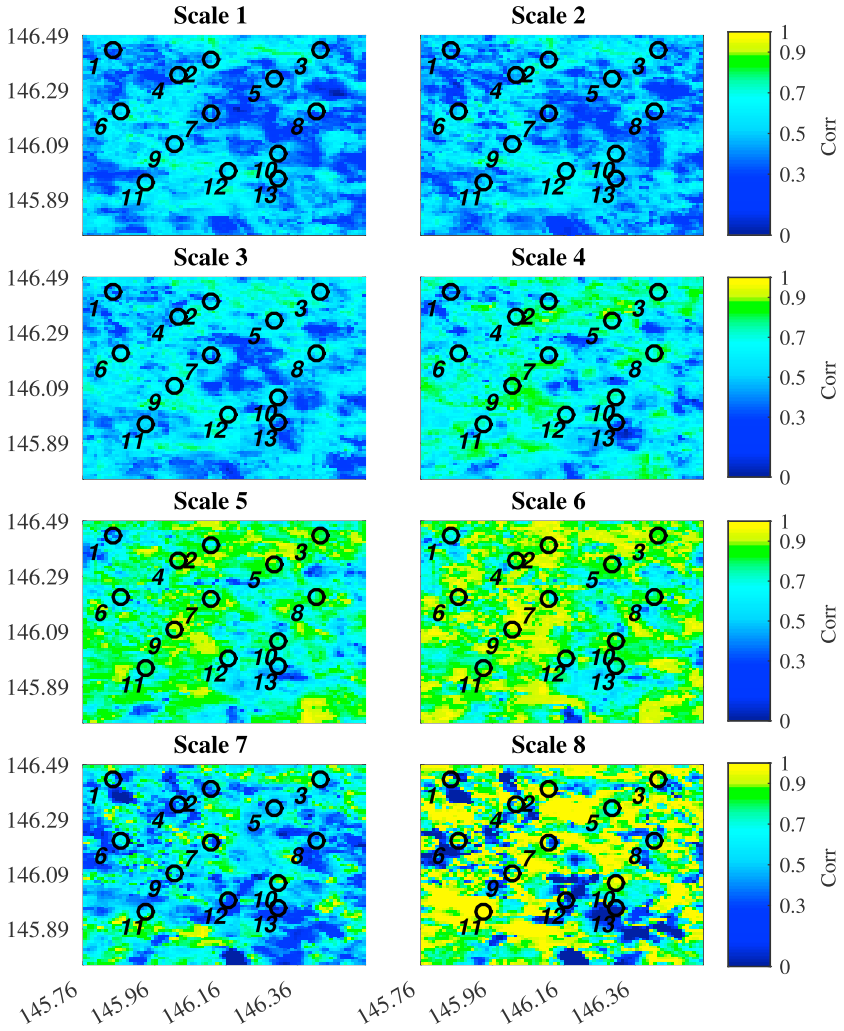

Figure 5. Maps of temporal correlation between each pixel time series and the field-average time series of the in situ-DIS data set. Values are calculated on detail series. Color code is bounded between 0 and 1, although negative correlation values exist.

The largest scales (16–64 days) deserve special attention. First, we recall that the relative positions between the lines change in Figure 4. This justifies the separate evaluation of spatial representativeness per timescale. For example, location 1 is a good option if we are interested in seasonal changes (64 day scale), but it is not for week-scale applications (8 and 16 day scales). Second and most importantly, the seasonal 64 days scale is the scale that exhibits the largest areas with correlation very close to 1: the most representative series exhibits ~40% of the area with a correlation above 0.9 (Figure 4). However, there are some locations that have extremely small representativeness areas (location 13) while others have extremely large ones (locations 9 and 10).

In order to investigate deeper, Figure 5 presents the correlation maps derived for the FAvg series, prior to the calculation of the CArea percentages for this series. It shows the same overall trend of increasing representativeness with timescale, including the correlation drop at the 32 day scale explained before. It also corroborates that at the 64 day scale, locations can be either highly representative of footprint SM (correlation close to 1, in yellow) or not at all (correlation <0.5, in dark blue). Additional experiments (not included here) showed that concurrent heterogeneities in precipitation synchronization and texture affected seasonal timescales, which can explain the observed dispersion in representativeness. From this, we conclude that the seasonal component of SM is made up of standalone seasonal elements (vegetation growing cycle, temperature trends, etc.) along with the integration over time of smaller timescale components, like short-time precipitation events and surface memory.

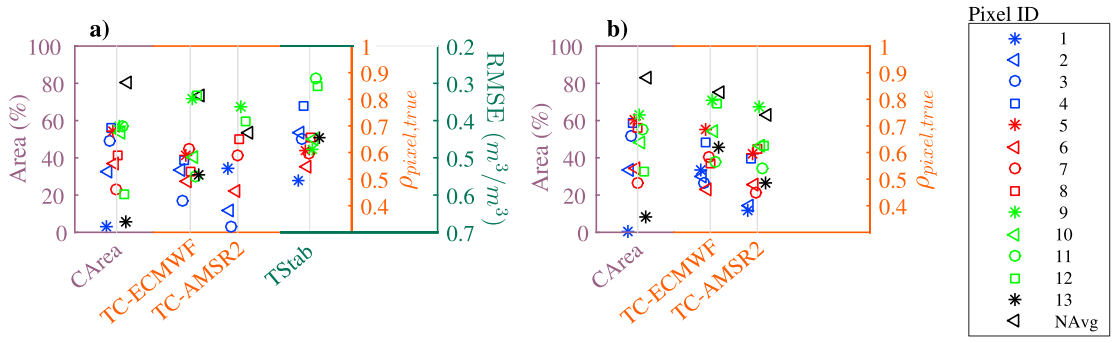

Figure 6. Representativeness values (vertical axis) from different methods (horizontal axis) for different pixels of the in situ-DIS Yanco data set. The methods are applied to (a) full series and to (b) detrended series (components >32 days are removed). The CArea correlation threshold is 0.55.

The results presented in this section solve the apparent opposition between the detrending in TC studies and the conclusions in Su and Ryu (2015) about seasonal scales that was mentioned in the introduction. Both Figures 4 and 5 reveal that, at seasonal timescales, both situations coexist: some locations exhibit important differences with respect to the footprint time series, as suggested in TC studies, but also a large number of locations exhibit good synchronization, as proposed by Su and Ryu (2015). Finally, we have also shown that time and spatial scales are connected in the model-based Little Washita and Yanco data sets. We hope to find similar behavior in actual in situ series (section 4.3), given that both model data sets are dependent on measured in situ data.

4.2. Intercomparison of Methods for Spatial Representativeness Assessment

Herein, we describe the second step of our investigation, which is dedicated to finding the best methods for assessing spatial representativeness of SM data sets, especially when SM time series are decomposed in timescales. To this end, we compare the performances of TStab, TC, CArea, and WCor methods when applied to the Yanco in situ-DIS data set for the 6 month period from September 2014 to March 2015. Because of the CArea method, the area of study includes all the stations plus a 0.05° extension to avoid border effects in peripheral stations. The TC triplets are made up of one local-support data set (one in situ-DIS series) and two large-support data sets (the SMOS data set and either the AMSR2 or the ECMWF data set).

4.2.1. Original Series

Figure 6a shows the spatial representativeness values obtained with each method on each selected location (pixel). The vertical axis is oriented from small to large representativeness, from bottom to top. Results are grouped per method: at the left, the CArea percentages; in the middle, the TC correlation $\rho_{\text{pixel,true}}$ values; and at the right, the TStab RMSE values (in reverse vertical-axis order). Some locations (markers) are missing from the TC groups because the preliminary test on the error variances (section 2.2.2) gave a negative value. This can be due to temporal biases, which can cause an imbalance between the data set variance and the product of covariances (equation (9)). TStab exhibits the largest disagreements with respect to the other methods. In agricultural sites, human decisions (cropping and irrigation) undermine TStab performances because they affect the temporal stability of the spatial distribution of SM (Yee et al., 2016).

In Figure 6a, the ranking of the locations in terms of representativeness is not the same for CArea and TC methods. Moreover, the values of the two TC variants are not coincident in general, although they both assign the largest values to the network average and pixels 9 and 12. All these differences could be induced by seasonal biases. Typically, TC studies removed the 30 day average component in order to have more chances to fulfill TC requirements (e.g., Chen et al., 2016; Miralles et al., 2010). In our case, we take advantage of the wavelet decomposition technique to provide a detrended triplet where variations larger than 32 days are removed. Figure 6b shows the representativeness scores of the detrended series. The ordering of the locations is more similar for the two TC variants than in Figure 6a. The wavelet-based detrending is beneficial because AMSR2 was positively biased during the first half of the period (not shown here). This can be due to C-band being more sensitive to vegetation and atmospheric factors than L-band. However, detrending does not prevent the TC and the CArea methods to provide very different results (Figure 6b). They both agree in

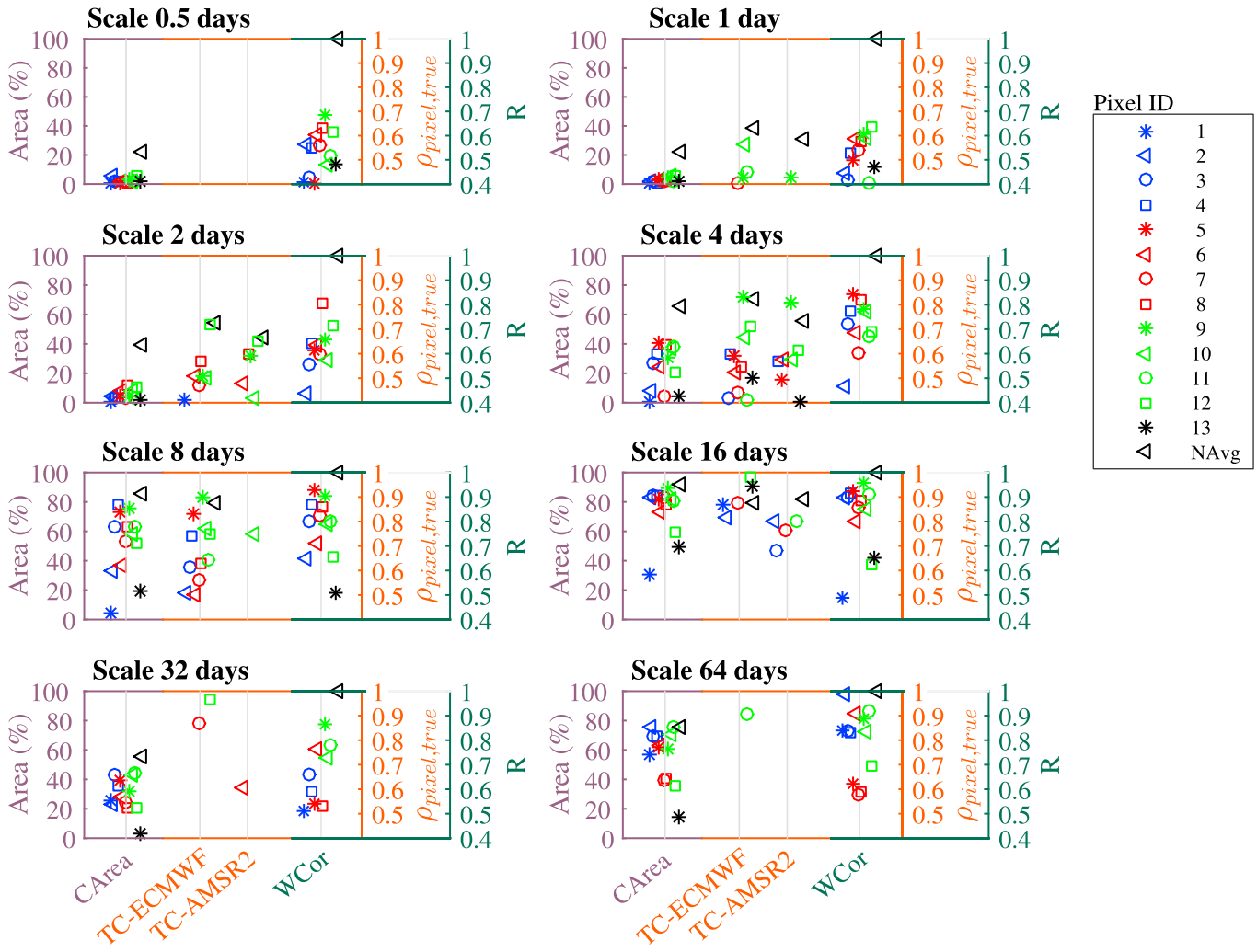

Figure 7. Spatial representativeness values from CArea, TC, and WCor methods for different pixels of the in situ-DIS Yanco data set, per timescale. The CArea correlation threshold is 0.55.

attributing more spatial representativeness to the network average and locations 9, 5, 4, 10, and 8, while smaller spatial representativeness to locations 1, 2, 6, and 7, but still some locations like 12, 13, and 3 exhibit large discrepancies. This reveals that detrending improves TC performance, but it does not succeed by itself to ensure that TC conditions are perfectly fulfilled.

4.2.2. Timescale Decomposed Series

The methods presented show significant differences in performance depending on whether some timescales, especially the seasonal one, are removed or not. Herein, we study the phenomenon in more detail at all timescales. The decomposition in timescales allows using the WCor approach, which compares the series of the selected pixels with the series of their spatial average (NAvg), on a per-timescale basis. In Figure 7, each plot contains the representativeness scores obtained with the different methods, including WCor, at a different timescale. There is a large absence of TC scores at the half-day, 1, 32, and 64 day scales. This is either because they are off vertical axis limits or because they fail the TC preliminary tests (e.g., most of the times the correlations between the data sets were too low, below 0.5, not shown here).

In Figure 7, the relative ranking of TC values differ to a great extent from that of the WCor and CArea values. Considering only the ECMWF-based configuration of the TC scores, the highest concordance between TC and WCor rankings occurs at the 8 day scale. The mismatch at larger scales (≥16 days) can be explained because the number of independent samples is drastically reduced due to wavelet filtering. The length of the series (366 samples) is already lower than TC recommendations: around 500 samples are needed for

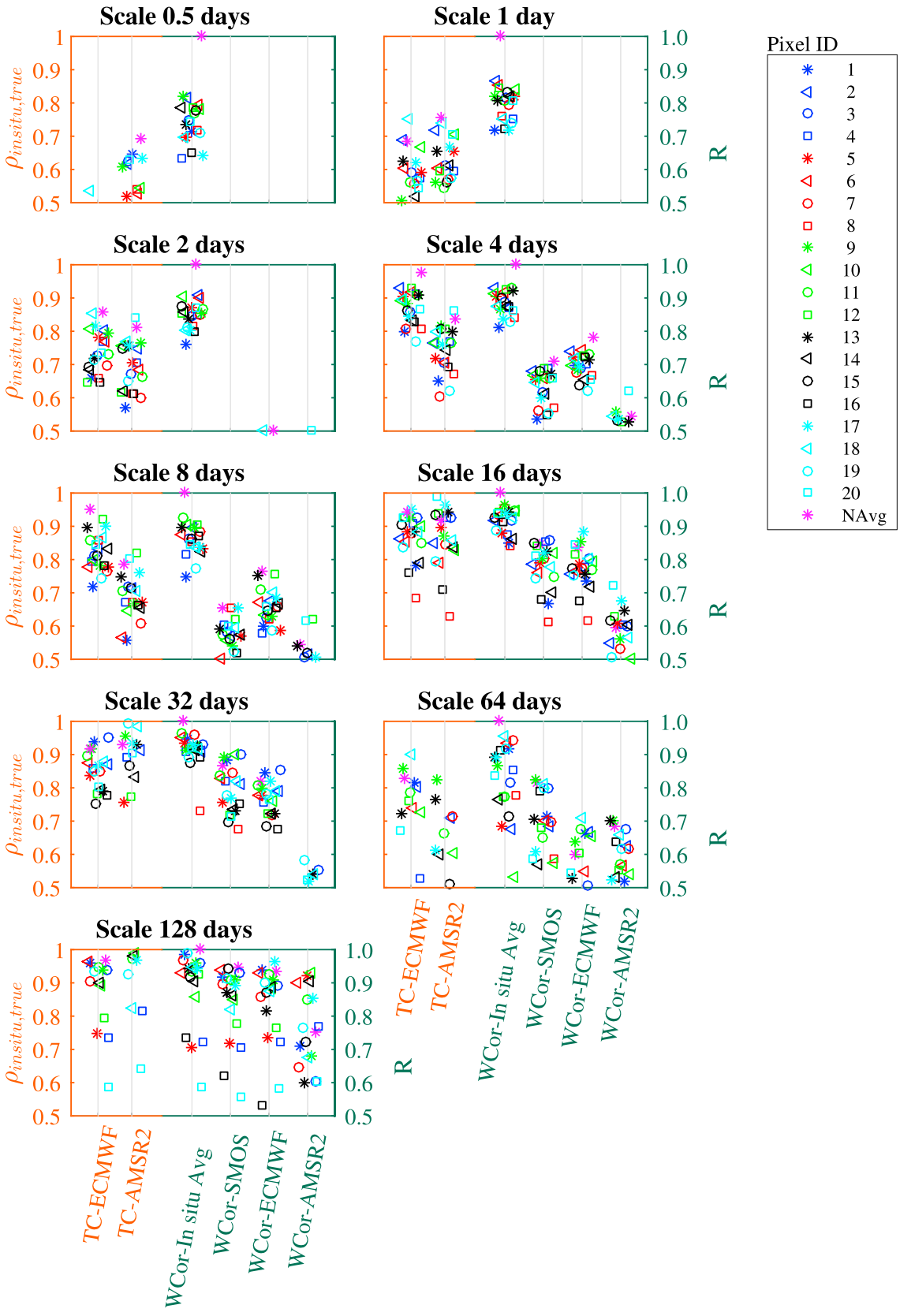

Figure 8. Spatial representativeness of Little Washita stations per timescale, evaluated with different TC and WCor methods for the 2 year period from July 2012 to July 2014.

error variances $\sigma^2_{\varepsilon_k}$ estimated with low uncertainty (11%; Zwieback et al., 2012). The mismatch at small scales (≤2 days) is probably due to the very low correlation between the data sets, which hampers the validity of the linear model assumption. All these suggest that TC should be applied neither to too short series nor to the shortest timescales.

Finally, the WCor and CArea methods give consistent results: the ranking of the locations is similar for all timescales. This is significant since the fact that a location correlates well/badly with the rest of locations (CArea) does not imply that it correlates well/badly with the network average (WCor), and vice versa: the correlation between the average and a point series cannot be simply summarized as the average of point-to-point correlation values. From this we conclude that WCor is a robust method for the evaluation of spatial representativeness on a per-timescale basis.

4.3. Spatial Representativeness Assessment of In Situ Series

This last section of results investigates whether the conclusions reached on modeled SM data apply to true in situ series, concretely those of the Little Washita network. The CArea method will no longer be applied since the spatial sampling is not sufficiently dense. The WCor method will be also tested on other large-support data sets different from the in situ average (SMOS, AMSR2, and ECMWF). It will allow exploring whether WCor could be applied to sparse networks (a single in situ station per footprint). The 2 year period from July 2012 to July 2014 is selected.

The results of the WCor and TC methods are presented in Figure 8. In contrast to the in situ-DIS Yanco case (section 4.2), much more TC scores are present, which is due to the larger number of samples. Figure 8 confirms the connection between time scales and spatial scales described in section 4.1: spatial representativeness increases with the timescale and the largest timescales (64 and 128 days) present the largest scatter in representativeness values. However, a drop in representativeness scores appears at the 64 day scale and concerns all the method configurations except the WCor-in situ avg. The most likely explanation is that the Little Washita network covers only half of the surface of the satellite footprints. As a consequence, the in situ series should present similar differences with respect to the satellite products in terms of precipitation and surface memory, and as explained in section 4.1, these elements can cause decorrelation in the 32 and 64 day scales.

Is the gap filling the root cause of the low representativeness scores at subweekly scales? According to the previous section, the gap filling in the point and average in situ series has a marginal effect. In addition, in this section we evaluated its effect on the large scale data sets. The procedure consisted in setting the large-scale data set gaps in the in situ series and computing the scores again. In the case of WCor, we observed that at scales smaller than 4 days, the experiment induced a small reduction in variance and an increase in correlation of between 0.05 and 0.2. According to these results, the gap filling does not change the relative scores presented in Figure 8 and in this study in general: the scores at scales smaller than 4 days remain much lower than those of larger timescales, even after taking into account the correlation increase due to gap filling.

When TC and WCor approaches are compared, similarities are found by groups (Figure 8): ECMWF-based TC results match well with the WCor results when the large-support data set is either the in situ average, SMOS, or ECMWF (first group), while AMSR2-TC values match well with the WCor-AMSR2 values (second group). This highlights that both TC and WCor methods have a high sensibility to the choice of the large-support data set. Two main features can explain the differences between the first and the second group. First, the gaps and the sensing time of AMSR2 series are different to those of the second group. Second, the interpolation of the custom ECMWF data set and its use as first guess in the SMOS retrieval system could foster similarity with SMOS-based scores. However, at the view of recent analyses of both products (Kerr et al., 2016), the SMOS retrievals are independent of ECMWF values.

The TC-WCor consistency is lost at the 64 day scale for the first group and at the 32 day scale for the second group. This is probably caused by a poorer performance of the TC method due to the reduction in the number of independent samples along with a correlation decrease between the data sets at those particular scales. This can be seen in Figure 9, where the correlation between the data sets is shown. We also observe that the higher correlation values for the first group at the 128 day scale (Figure 9a) seems related to the good consistency between WCor and TC results at this scale in Figure 8. For example, both methods designate stations 3, 11, 14, 15, 17, and 19 as the most representative and stations 2, 4, 5, 8, 16, and 20 as the least representative ones.

SMOS and ECMWF WCor results are the most similar to the in situ-avg WCor scores (Figure 8), so we consider necessary to examine them in more detail. First, SMOS- and ECMWF-based correlations are very low (<0.5)

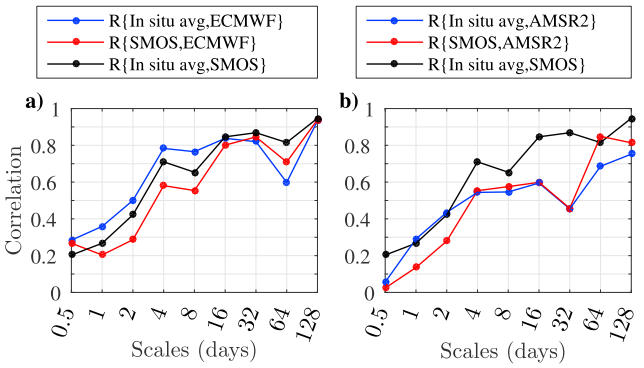

Figure 9. Correlation between decomposed series (detail series) of the Little Washita data sets: (a) the TC ECMWF-based triplet and (b) the TC AMSR2-based triplet. For clarity, only the in situ average series is present as in situ data set.

at the first three scales (0.5–2 days), while the in situ-avg, correlations are higher than 0.6. In the case of satellite data sets, this could be due to high-frequency noise, but not in the case of models like ECMWF that are governed by a smoother model structure. Another more likely explanation is related to the spatial support: the spacing between the in situ stations is larger than the correlation length of SM, which ranges between some meters to some hundreds of meters (De Lannoy et al., 2006; Western et al., 2004; Western et al., 1998). As a consequence, the in situ average is computed with an undersampled surface, which misses small spatial scale phenomena, while satellite sensors observe a continuous sampled surface. Moreover, satellite sensors estimate SM from the energy integrated over the footprint, which is not necessarily equal to the integral of SM due to nonlinearities in the models and in the scaling of parameters (Crosson et al., 2010; Crow et al., 2001). From this we conclude that the smallest timescales (≤2 days) are not good choices to validate satellite estimates given the large geophysical mismatch between satellite and in situ measurements.

Regarding the middle scales (4–16 days), the ranking of ECMWF-WCor is more similar to the in situ-avg ranking than the SMOS one (Figure 8), which we attribute to SMOS observational noise. However, at last scales (32–128 days) we observe the opposite. Therefore, we consider SMOS as a good large-support data set to be used for spatial representativeness assessment in the Little Washita region, especially at the month and seasonal scales.

5. Conclusions

Satellite surface SM products are often validated with ground samples by direct comparison, despite the different spatial supports of the two data sets (~50 km and a few centimeters, respectively). Ground samples can represent areas larger than their measurement support. The representativeness area may vary with the timescale (Entin et al., 2000). This study sought to investigate the connections between SM spatial scales and timescales within typical coarse scale satellite footprint-size areas. For this purpose, we evaluated the spatial representativeness of different locations at a range of timescales with various methods: triple collocation (TC), temporal stability analysis (TStab), the percentage of correlated area (CArea), and a new proposed approach consisting in wavelet-based correlations (WCor).

The comparison of the four approaches revealed that TStab, although applicable to SM absolute values, could not be applied to wavelet decomposed series because of their multiple zero crossings. TC could not give any results or gave results that were not consistent with the other methods under two situations: at short timescales (0.5–2 days), because the correlation between the data sets was too low, and at larger timescales (larger than 8 days in the case of 6 month series and larger than 32 days in the case of 2 year series), because the number of independent samples was too low after wavelet filtering. CArea and WCor results were consistent in general. WCor is less sensitive to the spatial sampling density than CArea, so it is a robust method for in situ networks that moreover requires less restrictive conditions than the three other approaches presented.

By applying TC, CArea, and WCor to modeled and true in situ time series in the Little Washita watershed and to spatialized SM data in the Yanco area, we found that SM spatial and timescales were connected. The series were sampled every 0.5 days. Precipitation and irrigation were found responsible of small representativeness areas at small timescales (0.5–2 days). As the timescale increased from 0.5 days to 128 days, the spatial representativeness scores tended to increase as well; however, they became more scattered. This was explained by different geophysical factors. First, desynchronizations in precipitation were propagated to larger timescales, preventing representativeness to regularly increase at some locations. Second, we observed that the seasonal scale did not only include seasonal signals (vegetation growth, temperature trends, etc.) but also the temporal integration of precipitation and soil memory responses from short and medium timescales.

This is, to our knowledge, the first comprehensive investigation on the connection between SM spatial and timescales within the satellite footprint (~50 km). It has revealed that time decompositions along with the WCor method are promising tools for improving satellite validation and modeling of surface soil moisture. At small timescales (below 4 days), the spatial scale mismatch between satellite/model series (SMOS,

AMSR2, and ECMWF) and in situ series was found extremely large and similar for all stations. Therefore, we suggest not taking into account these timescales in the validation of satellite products. At the seasonal scale, some locations were observed very similar to the footprint support series, while some others were very different. This explained why in some previous studies seasonal scales were found similar for both in situ and satellite series (e.g., Su & Ryu, 2015), while in TC studies, they were supposed intrinsically different so seasonal detrending was applied (e.g., Gruber et al., 2016). Finally, the findings of this study can contribute to other SM applications like downscaling or modeling: multiscale algorithms can be built based on the specific interactions at each time and spatial scale. Given its timescale dependence, spatial variability should be addressed differently depending on the timescale.

Acknowledgments
This study was financially supported by the "Terre, Océan, Surfaces Continentales, Atmosphère" and the CATDS programs of the "Centre National d'Études Spatiales" (CNES, France). USDA is an equal opportunity provider and employer. Soil moisture datasets accessed for this study are publicly available and the respective sources are listed in section 3 of this article. The authors acknowledge the USDA ARS for providing the elementary watershed information and the Murrumbidgee monitoring network, whose initial setup and maintenance was funded by the Australian Research Council (DP0343778, DP0557543) and by the CRC for Catchment Hydrology. The authors would like also to thank Robert Parinussa, Richard de Jeu and Robin van der Schalie (VUA) who produced and provided the AMSR2 LPRM soil moisture data sets to us.

References

Al Bitar, A., Leroux, D. J., Kerr, Y. H., Merlin, O., Richaume, P., Sahoo, A. K., & Wood, E. F. (2012). Evaluation of SMOS soil moisture products over continental U.S. using the SCAN/SNOTEL network. *IEEE Transactions on Geoscience and Remote Sensing*, *50*(5), 1572–1586. https://doi.org/10.1109/TGRS.2012.2186581

Allen, P. B., & Naney, J. W. (1991). *Hydrology of the Little Washita River Watershed, Oklahoma: Data and analyses*. United States Department of Agriculture, Agricultural Research Service. ARS-90

Barford, L. A., Fazzio, R. S., & Smith, D. R. (1992). *An introduction to wavelets*. Palo Alto, CA: Hewlett-Packard Company.

Berger, R. A., & Sweney, A. B. (1965). Variance and correlation coefficients. *Research Quarterly. American Association for Health, Physical Education Recreation*, *36*(3), 368–370. https://doi.org/10.1080/10671188.1965.10614705

Bircher, S., Skou, N., Jensen, K. H., Walker, J. P., & Rasmussen, L. (2012). A soil moisture and temperature network for SMOS validation in western Denmark. *Hydrology and Earth System Sciences*, *16*(5), 1445–1463. https://doi.org/10.5194/hess-16-1445-2012

Blöschl, G., & Sivapalan, M. (1995). Scale issues in hydrological modelling: A review. *Hydrological Processes*, *9*(3-4), 251–290. https://doi.org/10.1002/hyp.3360090305

Cayan, D. R., & Georgakakos, K. P. (1995). Hydroclimatology of continental watersheds: 2. Spatial analyses. *Water Resources Research*, *31*(3), 677–697. https://doi.org/10.1029/94WR02376

Chaney, N. W., Roundy, J. K., Herrera-Estrada, J. E., & Wood, E. F. (2014). High-resolution modeling of the spatial heterogeneity of soil moisture: Applications in network design. *Water Resources Research*, *51*, 619–638. https://doi.org/10.1002/2013WR014964

Chen, F., Crow, W. T., Colliander, A., Cosh, M. H., Jackson, T. J., Bindlish, R., … Seyfried, M. S. (2016). Application of triple collocation in ground-based validation of soil moisture active/passive (SMAP) level 2 data products. *IEEE Journal of Selected Topics in Applied Earth Observations and Remote Sensing*, *10*(2), 489–502. https://doi.org/10.1109/JSTARS.2016.2569998

Chen, F., Crow, W. T., Starks, P. J., & Moriasi, D. N. (2011). Improving hydrologic predictions of a catchment model via assimilation of surface soil moisture. *Advances in Water Resources*, *34*(4), 526–536. https://doi.org/10.1016/j.advwatres.2011.01.011

Cho, E., Su, C.-H., Ryu, D., Kim, H., & Choi, M. (2017). Does AMSR2 produce better soil moisture retrievals than AMSR-E over Australia? *Remote Sensing of Environment*, *188*, 95–105. https://doi.org/10.1016/j.rse.2016.10.050

Colliander, A., Jackson, T. J., Bindlish, R., Chan, S., Das, N., Kim, S. B., … Yueh, S. (2017). Validation of SMAP surface soil moisture products with core validation sites. *Remote Sensing of Environment*, *191*, 215–231. https://doi.org/10.1016/j.rse.2017.01.021

Cornish, C. R., Bretherton, C. S., & Percival, D. B. (2006). Maximal overlap wavelet statistical analysis with application to atmospheric turbulence. *Boundary-Layer Meteorology*, *119*(2), 339–374. https://doi.org/10.1007/s10546-005-9011-y

Cosh, M. H., Jackson, T. J., Moran, M. S., & Bindlish, R. (2008). Temporal persistence and stability of surface soil moisture in a semi-arid watershed. *Remote Sensing of Environment*, *112*(2), 304–313. https://doi.org/10.1016/j.rse.2007.07.001

Cosh, M. H., Jackson, T. J., Starks, P. J., & Heathman, G. (2006). Temporal stability of surface soil moisture in the Little Washita River watershed and its applications in satellite soil moisture product validation. *Journal of Hydrology*, *323*(1-4), 168–177. https://doi.org/10.1016/j.jhydrol.2005.08.020

Crosson, W. L., Limaye, A. S., & Laymon, C. A. (2010). Impacts of spatial scaling errors on soil moisture retrieval accuracy at L-band. *IEEE Journal of Selected Topics in Applied Earth Observations and Remote Sensing*, *3*(1), 67–80. https://doi.org/10.1109/JSTARS.2010.2041636

Crow, W. T., Berg, A. A., Cosh, M. H., Loew, A., Mohanty, B. P., Panciera, R., … Walker, J. P. (2012). Upscaling sparse ground-based soil moisture observations for the validation of coarse-resolution satellite soil moisture products. *Reviews of Geophysics*, *50*, RG2002. https://doi.org/10.1029/2011RG000372

Crow, W. T., Drusch, M., & Wood, E. F. (2001). An observation system simulation experiment for the impact of land surface heterogeneity on AMSR-E soil moisture retrieval. *IEEE Transactions on Geoscience and Remote Sensing*, *39*(8), 1622–1631. https://doi.org/10.1109/36.942540

Daly, E., & Porporato, A. (2005). A review of soil moisture dynamics: From rainfall infiltration to ecosystem response. *Environmental Engineering Science*, *22*(1), 9–24. https://doi.org/10.1089/ees.2005.22.9

Daubechies, I. (1992). 6. Orthonormal bases of compactly supported wavelets. In *Ten lectures on wavelets* (pp. 167–213). Philadelphia, PA: Society for Industrial and Applied Mathematics. https://doi.org/10.1137/1.9781611970104.ch6

De Lannoy, G. J. M., Verhoest, N. E. C., Houser, P. R., Gish, T. J., & Van Meirvenne, M. (2006). Spatial and temporal characteristics of soil moisture in an intensively monitored agricultural field (OPE3). *Journal of Hydrology*, *331*(3-4), 719–730. https://doi.org/10.1016/j.jhydrol.2006.06.016

Douville, H. (2004). Relevance of soil moisture for seasonal atmospheric predictions: Is it an initial value problem? *Climate Dynamics*, *22*(4), 429–446. https://doi.org/10.1007/s00382-003-0386-5

Draper, C. S., Reichle, R. H., De Lannoy, G. J. M., & Liu, Q. (2012). Assimilation of passive and active microwave soil moisture retrievals. *Geophysical Research Letters*, *39*, L04401. https://doi.org/10.1029/2011GL050655

Draper, C. S., Walker, J. P., Steinle, P. J., de Jeu, R. A. M., & Holmes, T. R. H. (2009). An evaluation of AMSR-E derived soil moisture over Australia. *Remote Sensing of Environment*, *113*(4), 703–710. https://doi.org/10.1016/j.rse.2008.11.011

Drusch, M. (2007). Initializing numerical weather prediction models with satellite-derived surface soil moisture: Data assimilation experiments with ECMWF's integrated forecast system and the TMI soil moisture data set. *Journal of Geophysical Research*, *112*, D03102. https://doi.org/10.1029/2006JD007478

Entin, J. K., Robock, A., Vinnikov, K. Y., Hollinger, S. E., Liu, S., & Namkhai, A. (2000). Temporal and spatial scales of observed soil moisture variations in the extratropics. *Journal of Geophysical Research*, *105*(D9), 11,865–11,877. https://doi.org/10.1029/2000JD900051

Foufoula-Georgiou, E., & Kumar, P. (1994). *Wavelets in geophysics* (Vol. 4). San Diego, CA: Academic Press. https://doi.org/10.1016/B978-0-08-052087-2.50007-4

Goodwin, L. D., & Leech, N. L. (2006). Understanding correlation: Factors that affect the size of *r*. *The Journal of Experimental Education*, *74*(3), 249–266. https://doi.org/10.3200/JEXE.74.3.249-266

Graf, A., Bogena, H. R., Drüe, C., Hardelauf, H., Pütz, T., Heinemann, G., & Vereecken, H. (2014). Spatiotemporal relations between water budget components and soil water content in a forested tributary catchment. *Water Resources Research*, *50*, 4837–4857. https://doi.org/10.1002/2013WR014516

Gruber, A., Dorigo, W. A., Zwieback, S., Xaver, A., & Wagner, W. (2013). Characterizing coarse-scale representativeness of in situ soil moisture measurements from the International Soil Moisture Network. *Vadose Zone Journal*, *12*(2), 1–16. https://doi.org/10.2136/vzj2012.0170

Gruber, A., Su, C.-H., Zwieback, S., Crow, W. T., Dorigo, W. A., & Wagner, W. (2016). Recent advances in (soil moisture) triple collocation analysis. *International Journal of Applied Earth Observation and Geoinformation*, *45*, 200–211. https://doi.org/10.1016/j.jag.2015.09.002

Haar, A. (1910). Zur Theorie der orthogonalen Funktionensysteme. *Mathematische Annalen*, *69*(3), 331–371. https://doi.org/10.1007/BF01456326

Jackson, T. J., Cosh, M. H., Bindlish, R., Starks, P. J., Bosch, D. D., Seyfried, M. S., … Du, J. (2010). Validation of advanced microwave scanning radiometer soil moisture products. *IEEE Transactions on Geoscience and Remote Sensing*, *48*(12), 4256–4272. https://doi.org/10.1109/TGRS.2010.2051035

Jacobs, J. M., Mohanty, B. P., Hsu, E.-C., & Miller, D. (2004). SMEX02: Field scale variability, time stability and similarity of soil moisture. *Remote Sensing of Environment*, *92*(4), 436–446. https://doi.org/10.1016/j.rse.2004.02.017

Japan Aerospace Exploration Agency (JAXA) (2013). *GCOM-W1 "SHIZUKU" Data users handbook*. Ibaraki, Japan: JAXA.

Katul, G. G., Porporato, A., Daly, E., Oishi, A. C., Kim, H., Stoy, P. C., … Siqueira, M. B. (2007). On the spectrum of soil moisture from hourly to interannual scales. *Water Resources Research*, *43*, W05428. https://doi.org/10.1029/2006WR005356

Kerr, Y. H., Al-Yaari, A., Rodríguez-Fernández, N. J., Parrens, M., Molero, B., Leroux, D., … Wigneron, J.-P. (2016). Overview of SMOS performance in terms of global soil moisture monitoring after six years in operation. *Remote Sensing of Environment*, *180*, 40–63. https://doi.org/10.1016/j.rse.2016.02.042

Kerr, Y. H., Waldteufel, P., Richaume, P., Ferrazzoli, P., & Wigneron, J.-P. (2014). *SMOS level-2 processor soil moisture algorithm theoretical basis document (ATBD)*. Toulouse: SM-ESL (CBSA).

Kerr, Y. H., Waldteufel, P., Richaume, P., Wigneron, J.-P., Ferrazzoli, P., Mahmoodi, A., … Delwart, S. (2012). The SMOS soil moisture retrieval algorithm. *Geoscience and Remote Sensing*, *50*(5), 1384–1403. https://doi.org/10.1109/TGRS.2012.2184548

Kerr, Y. H., Waldteufel, P., Wigneron, J.-P., Martinuzzi, J. M., Font, J., & Berger, M. (2001). Soil moisture retrieval from space: The Soil Moisture and Ocean Salinity (SMOS) mission. *IEEE Transactions on Geoscience and Remote Sensing*, *39*(8), 1729–1735. https://doi.org/10.1109/36.942551

Kornelsen, K. C., & Coulibaly, P. (2013). McMaster Mesonet soil moisture data set: Description and spatio-temporal variability analysis. *Hydrology and Earth System Sciences*, *17*(4), 1589–1606. https://doi.org/10.5194/hess-17-1589-2013

Lauzon, N., Anctil, F., & Petrinovic, J. (2004). Characterization of soil moisture conditions at temporal scales from a few days to annual. *Hydrological Processes*, *18*(17), 3235–3254. https://doi.org/10.1002/hyp.5656

Legates, D. R., Mahmood, R., Levia, D. F., DeLiberty, T. L., Quiring, S. M., Houser, C., & Nelson, F. E. (2011). Soil moisture: A central and unifying theme in physical geography. *Progress in Physical Geography*, *35*(1), 65–86. https://doi.org/10.1177/0309133310386514

Lei, F., Crow, W. T., Shen, H., Parinussa, R. M., & Holmes, T. R. H. (2015). The impact of local acquisition time on the accuracy of microwave surface soil moisture retrievals over the contiguous United States. *Remote Sensing*, *7*(10), 13,448–13,465. https://doi.org/10.3390/rs71013448

Loew, A., & Schlenz, F. (2011). A dynamic approach for evaluating coarse scale satellite soil moisture products. *Hydrology and Earth System Sciences*, *15*(1), 75–90. https://doi.org/10.5194/hess-15-75-2011

Malbéteau, Y., Merlin, O., Molero, B., Rüdiger, C., & Bacon, S. (2016). DisPATCh as a tool to evaluate coarse-scale remotely sensed soil moisture using localized in situ measurements: Application to SMOS and AMSR-E data in southeastern Australia. *International Journal of Applied Earth Observation and Geoinformation*, *45*(Part B), 221–234. https://doi.org/10.1016/j.jag.2015.10.002

Martínez-Fernández, J., & Ceballos, A. (2005). Mean soil moisture estimation using temporal stability analysis. *Journal of Hydrology*, *312*(1-4), 28–38. https://doi.org/10.1016/j.jhydrol.2005.02.007

McColl, K. a., Vogelzang, J., Konings, A. G., Entekhabi, D., Piles, M., & Stoffelen, A. (2014). Extended triple collocation: Estimating errors and correlation coefficients with respect to an unknown target. *Geophysical Research Letters*, *41*, 6229–6236. https://doi.org/10.1002/2014GL061322

Merlin, O., Escorihuela, M. J., Mayoral, M. A., Hagolle, O., Al Bitar, A., & Kerr, Y. H. (2013). Self-calibrated evaporation-based disaggregation of SMOS soil moisture: An evaluation study at 3 km and 100 m resolution in Catalunya, Spain. *Remote Sensing of Environment*, *130*(2013), 25–38. https://doi.org/10.1016/j.rse.2012.11.008

Merlin, O., Rüdiger, C., Al Bitar, A., Richaume, P., Walker, J. P., & Kerr, Y. H. (2012). Disaggregation of SMOS soil moisture in southeastern Australia. *IEEE Transactions on Geoscience and Remote Sensing*, *50*(5), 1556–1571. https://doi.org/10.1109/TGRS.2011.2175000

Miralles, D. G., Crow, W. T., & Cosh, M. H. (2010). Estimating spatial sampling errors in coarse-scale soil moisture estimates derived from point-scale observations. *Journal of Hydrometeorology*, *11*(6), 1423–1429. https://doi.org/10.1175/2010JHM1285.1

Mittelbach, H., & Seneviratne, S. I. (2012). A new perspective on the spatio-temporal variability of soil moisture: Temporal dynamics versus time-invariant contributions. *Hydrology and Earth System Sciences*, *16*(7), 2169–2179. https://doi.org/10.5194/hess-16-2169-2012

Mladenova, I. E., Lakshmi, V., Jackson, T. J., Walker, J. P., Merlin, O., & de Jeu, R. A. M. (2011). Validation of AMSR-E soil moisture using L-band airborne radiometer data from National Airborne Field Experiment 2006. *Remote Sensing of Environment*, *115*(8), 2096–2103. https://doi.org/10.1016/j.rse.2011.04.011

Molero, B., Merlin, O., Malbéteau, Y., Al Bitar, A., Cabot, F., Stefan, V. G., … Jackson, T. J. (2016). SMOS disaggregated soil moisture product at 1 km resolution: Processor overview and first validation results. *Remote Sensing of Environment*, *180*, 361–376. https://doi.org/10.1016/j.rse.2016.02.045

Nicolai-Shaw, N., Hirschi, M., Mittelbach, H., & Seneviratne, S. I. (2015). Spatial representativeness of soil moisture using in situ, remote sensing, and land reanalysis data. *Journal of Geophysical Research: Atmospheres*, *120*, 9955–9964. https://doi.org/10.1002/2015JD023305

Orlowsky, B., & Seneviratne, S. I. (2014). On the spatial representativeness of temporal dynamics at European weather stations. *International Journal of Climatology*, *34*(10), 3154–3160. https://doi.org/10.1002/joc.3903

Owe, M., de Jeu, R. A. M., & Holmes, T. R. H. (2008). Multisensor historical climatology of satellite-derived global land surface moisture. *Journal of Geophysical Research*, *113*, F01002. https://doi.org/10.1029/2007JF000769

Pan, F., Peters-Lidard, C. D., & Sale, M. J. (2003). An analytical method for predicting surface soil moisture from rainfall observations. *Water Resources Research*, *39*(11), 1314. https://doi.org/10.1029/2003WR002142

Parinussa, R. M., Holmes, T. R. H., & de Jeu, R. A. M. (2012). Soil moisture retrievals from the WindSat spaceborne polarimetric microwave radiometer. *IEEE Transactions on Geoscience and Remote Sensing*, *50*(7), 2683–2694. https://doi.org/10.1109/TGRS.2011.2174643

Percival, D. B., & Walden, A. T. (2000). *Wavelet methods for time series analysis*. Cambridge, UK: Cambridge University Press. https://doi.org/10.1017/CBO9780511841040

Rodriguez-Iturbe, I. (2000). Ecohydrology: A hydrologic perspective of climate–soil–vegetation dynamics. *Water Resources Research*, *36*(1), 3–9. https://doi.org/10.1029/1999WR900210

Smith, A., Walker, J. P., Western, A. W., Young, R. I., Ellett, K., Pipunic, R. C., … Richter, H. (2012). The Murrumbidgee soil moisture monitoring network data set. *Water Resources Research*, *48*, W07701. https://doi.org/10.1029/2012WR011976

Stoffelen, A. (1998). Toward the true near-surface wind speed: Error modeling and calibration using triple collocation. *Journal of Geophysical Research*, *103*(C4), 7755–7766. https://doi.org/10.1029/97JC03180

Su, C.-H., & Ryu, D. (2015). Multi-scale analysis of bias correction of soil moisture. *Hydrology and Earth System Sciences*, *19*(1), 17–31. https://doi.org/10.5194/hess-19-17-2015

Su, C.-H., Zhang, J., Gruber, A., Parinussa, R. M., Ryu, D., Crow, W. T., & Wagner, W. (2016). Error decomposition of nine passive and active microwave satellite soil moisture data sets over Australia. *Remote Sensing of Environment*, *182*, 128–140. https://doi.org/10.1016/j.rse.2016.05.008

Vachaud, G., Passerat De Silans, A., Balabanis, P., & Vauclin, M. (1985). Temporal stability of spatially measured soil water probability density function. *Soil Science Society of America Journal*, *49*(4), 822. https://doi.org/10.2136/sssaj1985.03615995004900040006x

Vereecken, H., Huisman, J. A., Pachepsky, Y., Montzka, C., van der Kruk, J., Bogena, H. R., … Vanderborght, J. (2014). On the spatio-temporal dynamics of soil moisture at the field scale. *Journal of Hydrology*, *516*, 76–96. https://doi.org/10.1016/j.jhydrol.2013.11.061

Vinnikov, K. Y., Robock, A., Speranskaya, N. A., & Schlosser, C. A. (1996). Scales of temporal and spatial variability of midlatitude soil moisture. *Journal of Geophysical Research*, *101*(D3), 7163–7174. https://doi.org/10.1029/95JD02753

Vogelzang, J., & Stoffelen, A. (2012). Triple collocation, *EUTMETSAT report*.

Wagner, W., Naeimi, V., Scipal, K., de Jeu, R. A. M., & Martínez-Fernández, J. (2007). Soil moisture from operational meteorological satellites. *Hydrogeology Journal*, *15*(1), 121–131. https://doi.org/10.1007/s10040-006-0104-6

Wang, G., Garcia, D., Liu, Y. Y., de Jeu, R. A. M., & Johannes Dolman, A. (2012). A three-dimensional gap filling method for large geophysical data sets: Application to global satellite soil moisture observations. *Environmental Modelling and Software*, *30*, 139–142. https://doi.org/10.1016/j.envsoft.2011.10.015

Wang, J., Ge, Y., Heuvelink, G. B. M., & Zhou, C. (2015). Upscaling in situ soil moisture observations to pixel averages with spatio-temporal geostatistics. *Remote Sensing*, *7*(9), 11,372–11,388. https://doi.org/10.3390/rs70911372

Webster, R., & Oliver, M. A. (1992). Sample adequately to estimate variograms of soil properties. *Journal of Soil Science*, *43*(1), 177–192. https://doi.org/10.1111/j.1365-2389.1992.tb00128.x

Western, A. W., Blöschl, G., & Grayson, R. B. (1998). Geostatistical characterisation of soil moisture patterns in the Tarrawarra catchment. *Journal of Hydrology*, *205*(1-2), 20–37. https://doi.org/10.1016/S0022-1694(97)00142-X

Western, A. W., Zhou, S. L., Grayson, R. B., McMahon, T. A., Blöschl, G., & Wilson, D. J. (2004). Spatial correlation of soil moisture in small catchments and its relationship to dominant spatial hydrological processes. *Journal of Hydrology*, *286*(1-4), 113–134. https://doi.org/10.1016/j.jhydrol.2003.09.014

Wigneron, J.-P., Kerr, Y. H., Waldteufel, P., Saleh, K., Escorihuela, M. J., Richaume, P., … Schwank, M. (2007). L-Band Microwave Emission of the Biosphere (L-MEB) model: Description and calibration against experimental data sets over crop fields. *Remote Sensing of Environment*, *107*(4), 639–655. https://doi.org/10.1016/j.rse.2006.10.014

Yee, M. S., Walker, J. P., Monerris, A., Rüdiger, C., & Jackson, T. J. (2016). On the identification of representative *in situ* soil moisture monitoring stations for the validation of SMAP soil moisture products in Australia. *Journal of Hydrology*, *537*, 367–381. https://doi.org/10.1016/j.jhydrol.2016.03.060

Yilmaz, M. T., & Crow, W. T. (2014). Evaluation of assumptions in soil moisture triple collocation analysis. *American Meteorological Society*, *15*(3), 1293–1302. https://doi.org/10.1175/JHM-D-13-0158.1

Zwieback, S., Scipal, K., Dorigo, W. A., & Wagner, W. (2012). Structural and statistical properties of the collocation technique for error characterization. *Nonlinear Processes in Geophysics*, *19*(1), 69–80. https://doi.org/10.5194/npg-19-69-2012

Erratum

In the originally published version of this article there were errors in the acknowledgement section as well as within the body of the text. On page 6, in the last paragraph, the line "Two TC metrics are typically used x_k" should read "Two TC metrics are typically used to assess the errors of each dataset x_k". Additionally, In Equation 10, "true" should be a subscript, at the same level as the 'x' in the subscript. And in Equation 12, "j" should be at the same level as "i" in the subscript, not as "0".

Below, you will find the acknowledgment section as it should have read.

This study was financially supported by the "Terre, Océan, Surfaces Continentales, Atmosphère" and the CATDS programs of the "Centre National d'Études Spatiales" (CNES, France). USDA is an equal opportunity provider and employer. Soil moisture datasets accessed for this study are publicly available and the respective sources are listed in section 3 of this article. The authors acknowledge the USDA ARS for providing the elementary watershed information and the Murrumbidgee monitoring network, whose initial setup and maintenance was funded by the Australian Research Council (DP0343778, DP0557543) and by the CRC for Catchment Hydrology. The authors would like also to thank Robert Parinussa, Richard de Jeu and Robin van der Schalie (VUA) who produced and provided the AMSR2 LPRM soil moisture data sets to us.

These errors have since been corrected, and this version may be considered authoritative version of record.